The Retro-Reflector for the CHAMP Satellite: Final Design and Realization

Reinhart Neubert, Ludwig Grunwaldt, Jakob Neubert*)
GeoForschungsZentrum Potsdam, Div.1: Kinematics and Dynamics of the Earth
Telegrafenberg , D-14473 Potsdam, Germany
Tel.: (49)-331-288-1153, Fax.: (49)-331-288-1111, e-mail: neub@gfz-potsdam.de

Summary

The precise orbit determination of the CHAMP satellite will rely on the data of the onboard GPS receivers. It is expected that using these data short arc orbits can be determined to a precision of 1cm or even better. Therefore SLR data of the same precision are required to calibrate the GPS system in the initial phase of the project. During the overall CHAMP mission, SLR data will be useful in a composite database to strengthen the precise orbit determination.
The design philosophy and main properties of the reflector are described in [1]. The array is formed by four cube corner prisms mounted in a compact frame (Fig.1). This design ensures that only one prism is contributing to the signal in general, except for some cases (near culmination of the satellite for instance) where the signals of two prisms are interfering. However because of the small dimensions of the array the signature cannot be resolved by present SLR systems.
In this paper the final design and specifications of the retro- reflector are presented. In addition the method of adaptation to the effect of velocity aberration is described. Calculations of the diffraction patterns for different orientations are used for more precise estimates of the reflected signal energy. Measured far field diffraction patterns of the individual cube corner prisms are in reasonable agreement with the calculations. The method of precise range correction is considered.

Description of the Retro-Reflector

The cube corner prisms of the reflector are made from fused quartz glass according to the specifications of Tab.1. The reflecting surfaces are aluminum coated. The uncoated front face is slightly spherical to increase the diameter of the two lobes of the reflection pattern. The splitting into two lobes is caused by a slight offset of one of the dihedral angles.

Table 1: Specifications of the cube corner prisms

Vertex length	28 mm
Clear aperture of the front face	38 mm
Dihedral angle offset	-3.8“ (smaller than 90 deg)
Radius of curvature of the front face	+500 m (convex)
Index of refraction @ 532nm	1.461
Nominal separation of the far field maxima	24“
Nominal width of the far field peaks (20% intensity of max.)	10“

The prisms are cemented using soft silicon rubber into mounting flanges which are screwed to the frame, a regular 45°- pyramid (Fig.1 and Fig.2).
The cube corner prisms produce two-spot far field diffraction patterns. By proper orientation of the prisms it can be achieved that one of the lobes is directed to the apparent position of the station.

*) Fraunhofer Institute for Applied Optics Jena , now with Oerlikon-Contraves, Zuerich

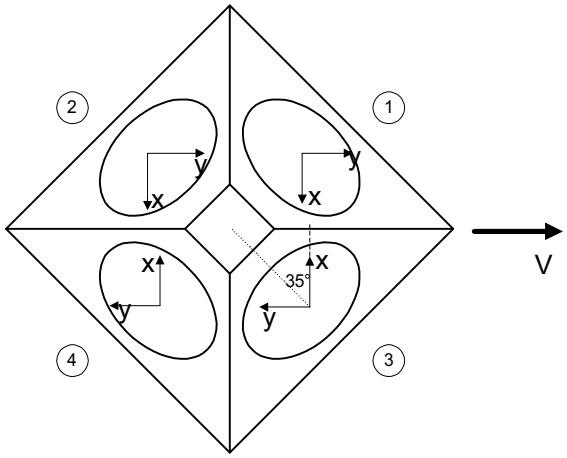

Fig.1: Schematic drawing of the array as seen from ground. The right hand arrow indicates the satellite velocity vector. The local coordinate systems for each prism (x-y) with x parallel to the projection of the non orthogonal edge are rotated by 35° as indicated.

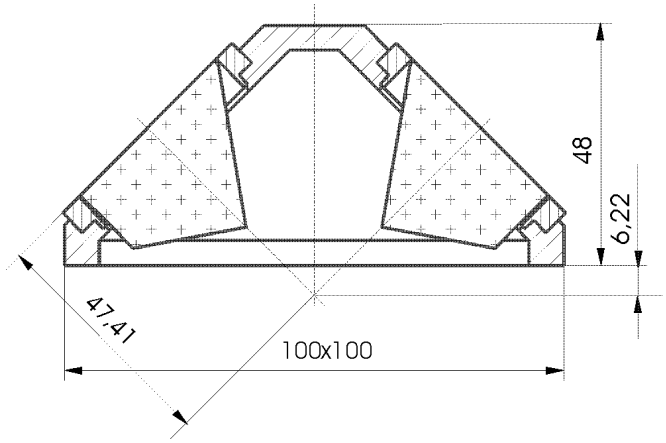

Fig.2: Sectional view of the array indicating the location of the reference point

Simulation of the Effects of Aberration and Diffraction on the Return Signal Strength

Both the far field diffraction pattern as well as the aberration vector are orientation dependent. Therefore an optimum aberration compensation can be achieved for a special orientation only. To find a reasonable compromise for all orientations we computed diffraction patterns for a set of orientations and determined the relative intensity received at the station.

The diffraction patterns were computed using the commercial software package ASAP [2...4]. A space fixed „laboratory" coordinate system was introduced. In the start configuration the front face of the prism is identical with the x-y- plane and the non-orthogonal edge of the prism is coplanar with x-z- plane. The different orientations to the incoming beam are realized by rotating the prism around the z-axis by the azimuth angle -Φ and then around the x- axis by the tilt angle -Θ. The optical field at z= 100 km is regarded as an approximation of the far field. Instead of angular coordinates x and y in meters are used in the representation of the far field data (see Appendix). For convenience , the far field patterns are rotated back by the angle Φ so that they always appear nearly symmetrical to the x-axis.

To estimate the intensity at the receiving telescope we need the apparent station position due to aberration in the same coordinate system. It depends on the orientation of the reflector relative to the satellite velocity vector. In our case the following relation holds:

$$A_x = 2 \cdot \frac{v}{c}\left(\frac{\sqrt{3}}{2} \cdot \sin(\Phi) \cdot \cos(\Phi) - \frac{\sqrt{3}}{2} \cdot \sin(\Phi) \cdot \cos(\Phi) \cdot \cos(\Theta) \mp \frac{1}{2} \cdot \sin(\Phi) \cdot \sin(\Theta) \right)$$

$$A_y = 2 \cdot \frac{v}{c}\left(\frac{\sqrt{3}}{2} \cdot \sin^2(\Phi) + \frac{\sqrt{3}}{2} \cdot \cos^2(\Phi) \cdot \cos(\Theta) \pm \frac{1}{2} \cdot \cos(\Phi) \cdot \sin(\Theta) \right) \qquad \text{Eq.1}$$

where ν is the orbital velocity and c the velocity of light. The two signs of the last term for A_x and A_y are due to the ascending (prism 1 or 3 in Fig.1) or descending part of the pass (prism 2 or 4 in Fig.1) respectively.

Using this relation, the relative intensity at the station has been obtained for a set of orientations. It can be converted into the expected number of photoelectrons for a typical SLR station. The results are tabulated in Tab.2 and graphically represented in Fig. 3 and 4 (prism

No.1 only). The graphs are using a different coordinate system to describe the beam direction. The X axis is parallel to the satellite velocity and the Z axis is Nadir direction. The Y axis completes to a right handed system. The scales in the Figures are corresponding to the components of a unit vector from the satellite to the station. Fig. 3 is a contour map of the expected number of photoelectrons whereas Fig.4 represents the elevation angle in the same coordinate system. It can be seen that multi photoelectron signals are expected for elevation angles above 20°.

Table 2.: Return Strength versus orientation of a single prism at 470 km orbital altitude for a station with the following parameters:
laser divergency $3 \cdot 10^{-4}$ rad, laser energy : 5 mJ,
receiver telescope diam. 40cm
receiver transmittance: 20%, quantum efficiency: 5%

		ascending			descending		
Θ	Φ	Elev.	Flux	pe	Elev.	Flux	pe
0	0	40.6	0.028100	181.9	40.6	0.028100	181.9
10	0	46.5	0.018300	193.2	33.1	0.022400	65.2
10	30	50.8	0.020700	293.9	38.5	0.028700	152.5
10	60	51.9	0.023000	351.8	44.5	0.031200	283.2
10	90	49.5	0.028800	377.6	49.5	0.028700	376.3
10	120	44.5	0.031200	283.2	51.9	0.022800	348.7
10	150	38.5	0.028700	152.5	50.8	0.020600	292.5
10	180	33.1	0.022300	64.9	46.5	0.018300	193.2
10	210	29.4	0.017600	31.6	40.7	0.017500	113.8
10	240	28.5	0.017300	27.0	34.9	0.017600	63.1
10	270	30.5	0.017400	36.0	30.5	0.017300	35.8
10	300	34.9	0.017600	63.1	28.5	0.017200	26.8
10	330	40.7	0.017700	115.1	29.4	0.017800	32.0
20	0	50.3	0.007830	108.2	24.0	0.008870	6.6
20	30	59.9	0.007500	175.1	34.6	0.016700	58.2
20	60	62.9	0.010800	286.3	46.3	0.018400	192.0
20	90	57.0	0.015300	311.2	57.0	0.015100	307.1
20	120	46.3	0.018300	190.9	62.9	0.010700	283.6
20	150	34.6	0.016600	57.9	59.9	0.007390	172.5
20	180	24.0	0.008860	6.6	50.3	0.007860	108.7
20	210	15.9	0.007030	0.8	38.7	0.008980	48.4
20	240	13.4	0.006290	0.3	27.5	0.007350	9.9
20	270	18.3	0.007100	1.6	18.3	0.006990	1.5
20	300	27.5	0.007500	10.1	13.4	0.006230	0.3
20	330	38.7	0.009040	48.7	15.9	0.006960	0.8
30	0	51.7	0.002330	35.1	11.4	0.002410	0.1
30	30	67.3	0.003150	98.2	29.0	0.004900	8.3
30	60	73.5	0.003430	126.9	45.8	0.006800	68.1
30	90	62.3	0.005570	144.0	62.3	0.005540	143.2
30	120	45.8	0.006840	68.5	73.5	0.003380	125.0
30	150	29.0	0.004920	8.3	67.3	0.003160	98.5
30	180	11.4	0.002450	0.1	51.7	0.002320	35.0
30	210	0.0	0.002170	0.0	34.8	0.003350	12.0
30	240	0.0	0.002810	0.0	18.0	0.002890	0.6
30	270	0.0	0.002760	0.0	0.0	0.002730	0.0
30	300	18.0	0.002910	0.6	0.0	0.002750	0.0
30	330	34.8	0.003380	12.1	0.0	0.002160	0.0
40	0	50.3	0.001670	23.1	0.0	0.000495	0.0
40	30	71.3	0.000449	15.7	21.6	0.000572	0.3
40	60	83.4	0.000642	27.8	43.0	0.000956	7.6
40	90	64.0	0.000867	24.0	64.0	0.000867	24.0
40	120	43.0	0.000945	7.5	83.4	0.000631	27.3
40	150	21.6	0.000574	0.3	71.3	0.000447	15.7
40	180	0.0	0.000494	0.0	50.3	0.001660	23.0
40	210	0.0	0.000852	0.0	29.3	0.000923	1.6
40	240	0.0	0.000801	0.0	0.0	0.000752	0.0
40	270	0.0	0.000809	0.0	0.0	0.000802	0.0
40	300	0.0	0.000751	0.0	0.0	0.000805	0.0
40	330	29.3	0.000914	1.6	0.0	0.000846	0.0

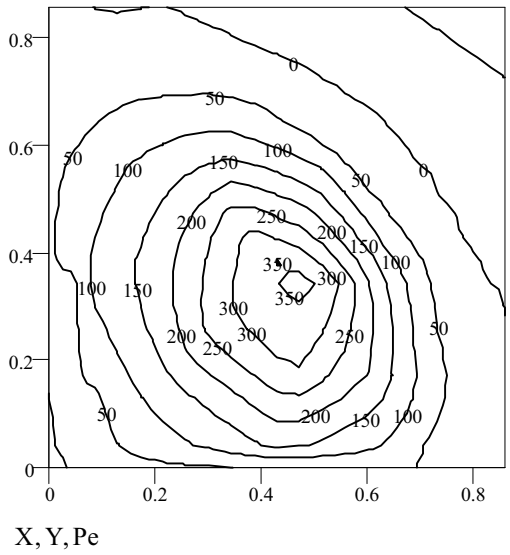

Fig.3: Expected pe number versus direction from satellite to station

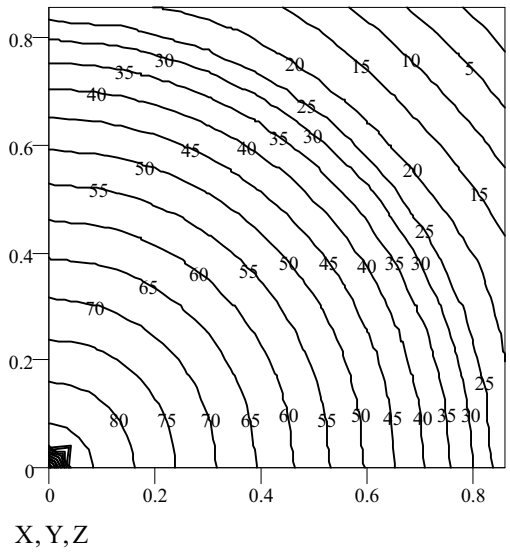

Fig.4: Elevation angle versus direction from satellite to station

In some directions (Θ,Φ) there is no real intersection of the line of sight with the (spherical) Earth. In these cases both the elevation as well as the number of photoelectrons are set to zero in Table 2.

Experimental test of the cube corner performance

The cube corner prisms have been produced by the manufacturer, Fa. Halle Nachf. Berlin, as close as possible to the specifications. After completion of the plane surfaces the dihedral angles were determined using a ZYGO interferometer in the double pass mode. The errors were close to the accuracy limit of the interferometer of about 0.2“. Then the front faces were spherically distorted to enlarge the width of the two far field spot to the desired value. In addition to the interferometric tests the far fields were observed directly using a collimator both with tungsten lamp as well as He-Ne laser illumination.

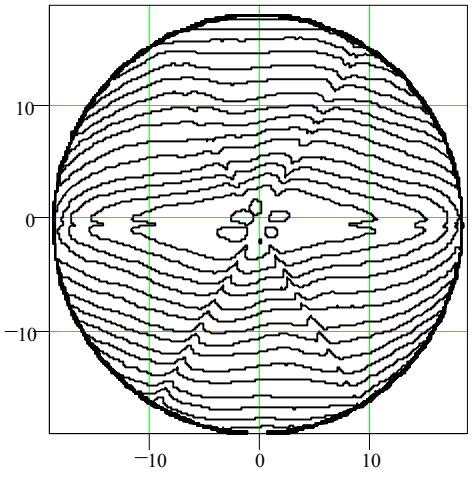

F

Fig.5: Wavefront of a sample prism
The phase difference between adjacent contours corresponds to 82 nm.

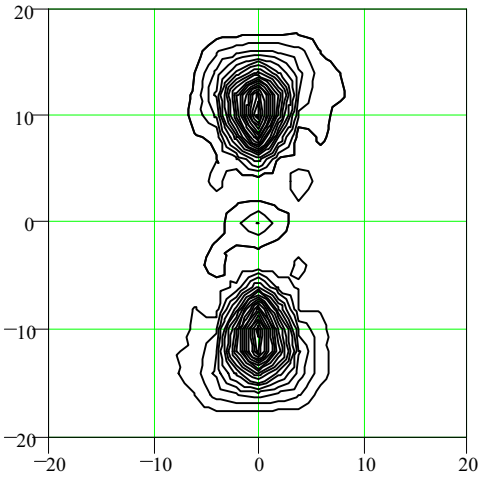

E

Fig.6 : Far field pattern computed by Fourier transform of the phase. The lowest level contour is at 5% of the maximum

Fig.7: Far field pattern observed directly using He-Ne laser illumination. The nonlinearity of the CCD and electronic system has not been corrected. This causes probably the slightly more extended spots compared to Fig.6.

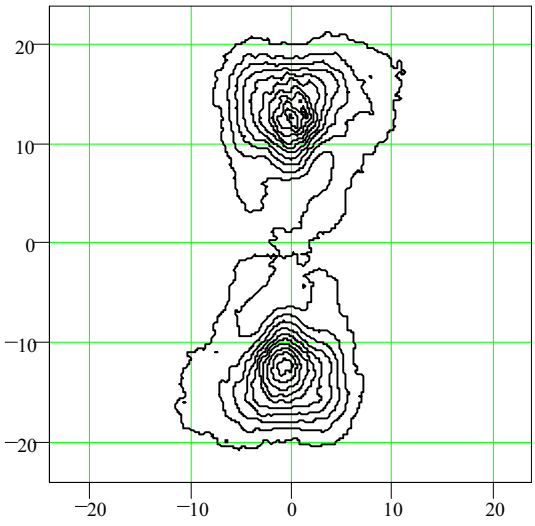

A2

The Range Correction

As a reference point of the array we are using the crossing point of the optical axes of the cube corner prisms. The range correction of a single cube corner referred to this point is given by the equation:

$$\Delta R = D \cdot \cos(\alpha) - L \cdot \sqrt{n^2 - \sin(\alpha)^2} \qquad \text{Eq.2}$$

where :

L: vertex length

D: distance of the prism front face from the reference point (D= 47.4 mm)

n: index of refraction

α: angle of incidence (relative to the normal to the front face)

The reference point is outside of the corpus of the reflector with a distance of 6.2 mm from the mounting plane (Fig.2).

The range correction ΔR has to be added to the measured range.

Eq.2 represents the ideal case if one prism is contributing to the signal. In the general case the weighted sum of the individual reflectors has to be computed:

$$\overline{\Delta R} = \frac{\sum_k S_k \cdot \Delta R_k}{\sum_k S_k} \qquad \text{Eq.3}$$

where the S_k and ΔR_k denote the relative intensities and range corrections of the individual reflectors respectively.

To represent the range correction according to Eq. 2 and Eq.3 graphically we introduce a satellite fixed coordinate system, with the x-axis parallel to the nominal flight direction and the z-axis parallel to the nominal nadir direction. In the following contour plot the relative intensities S_k depend mainly on the active area of the cube corners and the apparent position of the station in the far field diffraction pattern. To get a rough estimate, we neglect the influence of aberration and diffraction using the active area as a measure of the relative signal. The angular dependence of the active area of a metal coated cube corner can be approximated by:

$$S_k = \left(1 - \frac{\alpha_k}{0.85}\right)^2 \qquad \text{Eq.4}$$

where α_k is the angle of incidence for the prism No. k in radians .

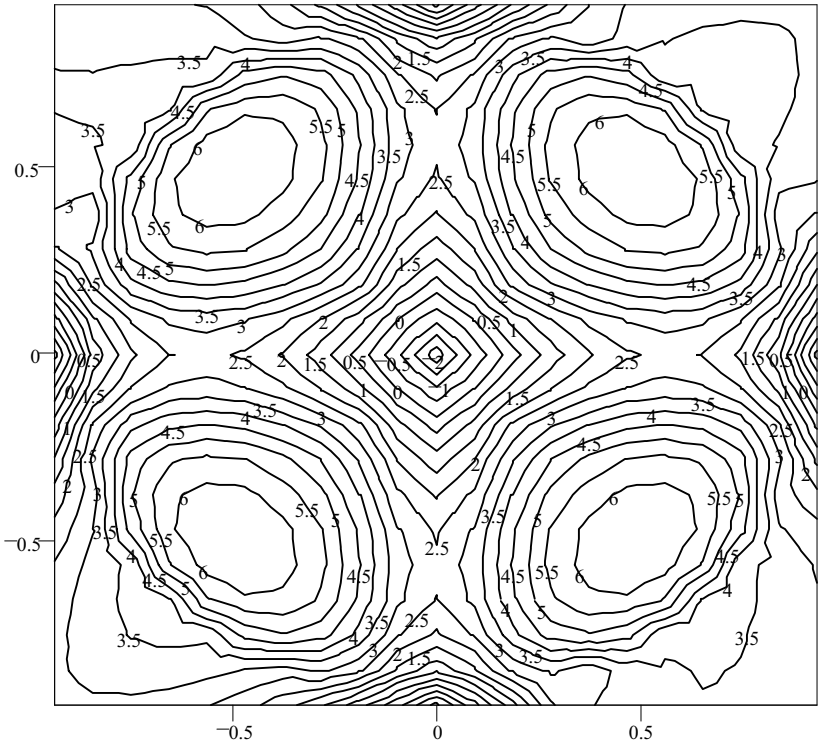

Fig.8: Contour map of the effective range correction. The plotting range corresponds to a nadir distance from zero to 70°. The independent variables X,Y are the components of the unit vector from the satellite to the station (direction of the reflected beam) whereas Z is the range correction in millimeters. The maxima correspond to normal incidence to one of the prisms.

As can be seen the variation of the range correction is below 1 cm. For many purposes the range correction may be replaced by the constant value $\Delta R = (5 \pm 2) mm$.

. The next level of approximation would be to use the range correction of the dominating prism with smallest angle of incidence, neglecting any crosstalk according to Eq.3. The error of such an approximation will be well below 1 mm.

To refer the measured range to the center of mass (CoM) of the satellite one has further to add the scalar product of the vector from the CoM to the reference point with the unit vector of the light direction. The attitude control of the satellite will ensure that this vector is always directed to Nadir within 2 degrees. The nominal distance of the array reference point from the CoM is 250 mm. This corresponds to a maximum error of the total range correction of 9 mm. However, the attitude dependent error can be corrected using the orientation data from the star sensors which will be made available.

References

[1] R.Neubert, Preliminary Design of the laser retroreflector for the CHAMP satellite, Proc.10th Workshop on Laser Ranging Instrumentation, Shanghai Nov.1996, p.216

[2] J.Neubert, calculation of the far field energy distribution of the CHAMP satellite retroreflector. Final report, Fraunhofer Institut für Angewandte Optik und Feinmechanik, Jena, 1997

[3] A.Greynolds, Propagation of Generally Astigmatic Gaussian Beams along Skew Ray Paths, Proc.SPIE: Diffractive Phenomena in Optical Engineering Applications 560 (1985), 33-50

[4] ASAP Online Reference, BRO Res. Inc., Tucson, Arizona USA

Appendix: Simulated Far Field Patterns for 0° and 40° Inclination

In this appendix we reproduce some results taken from Ref. [2].
As an example and a key to the meaning of the numbers appearing on the plots we show the far field pattern of an ideal retroreflector (no tilt, no front surface curvature) at normal incidence, which as expected very much reminds the Airy disc. The other plots refer to a cube corner prism as specified in Tab.1. The diffraction patterns at a distance of 100 km from the reflector are plotted. The lateral units are meters (corresponding to 10 microrad.)

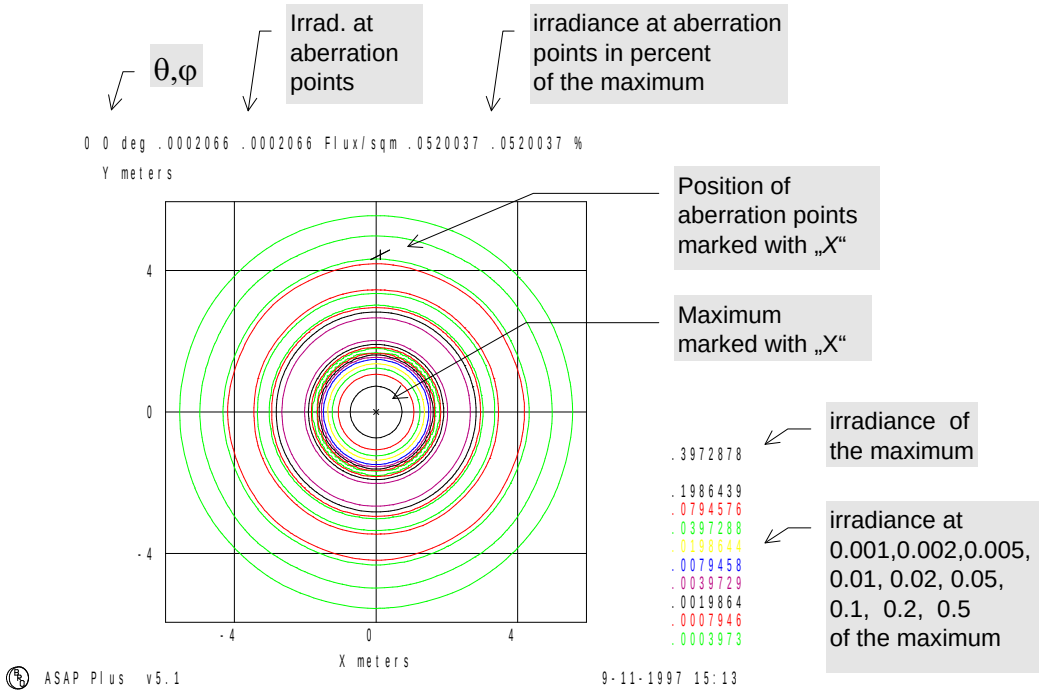

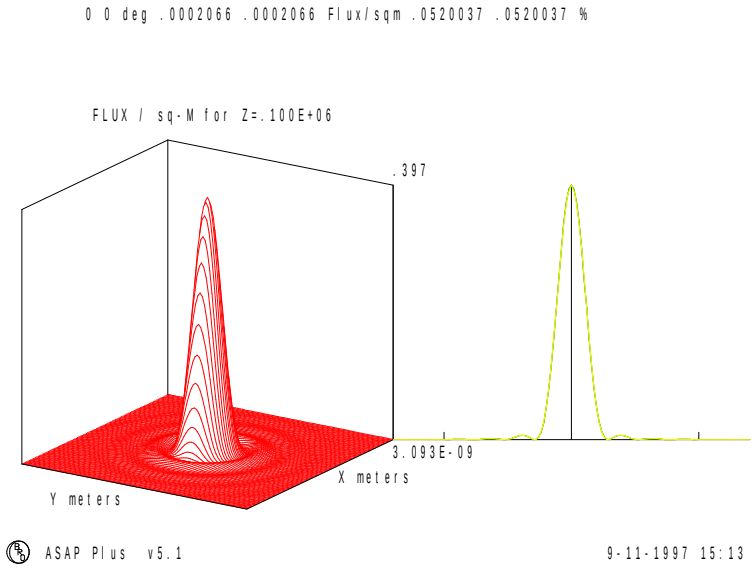

0 0 deg .0281228 .0281228 Flux/sqm 68.42227 68.42227 %

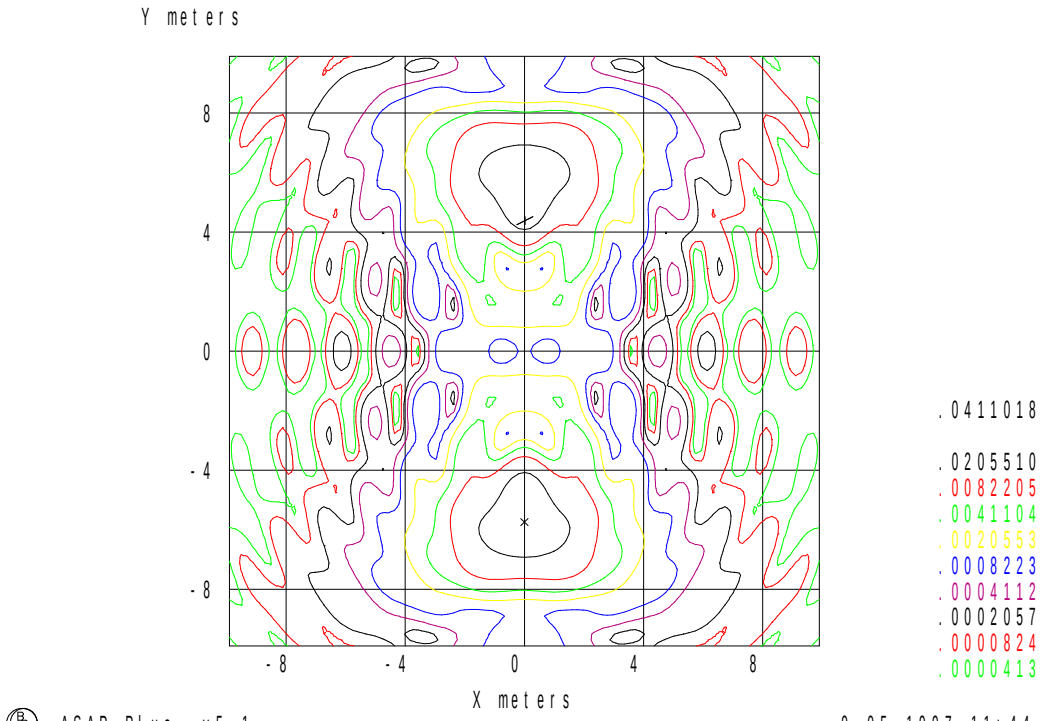

ASAP Plus v5.1 9-05-1997 11:44

0 0 deg .0281228 .0281228 Flux/sqm 68.42227 68.42227 %

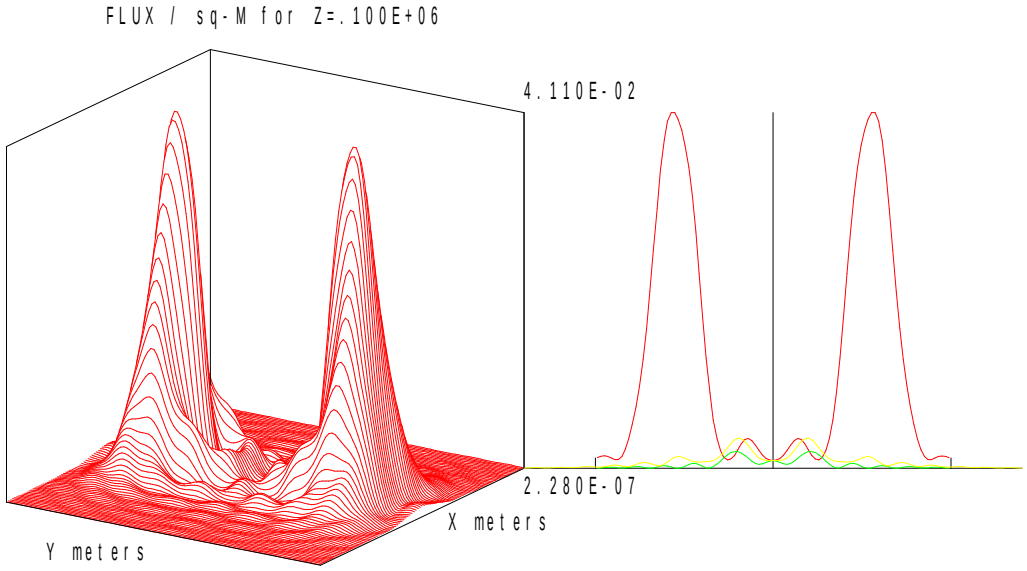

ASAP Plus v5.1 9-05-1997 11:44

40 90 deg .0008675 .0008676 Flux/sqm 61.62497 61.6356 %

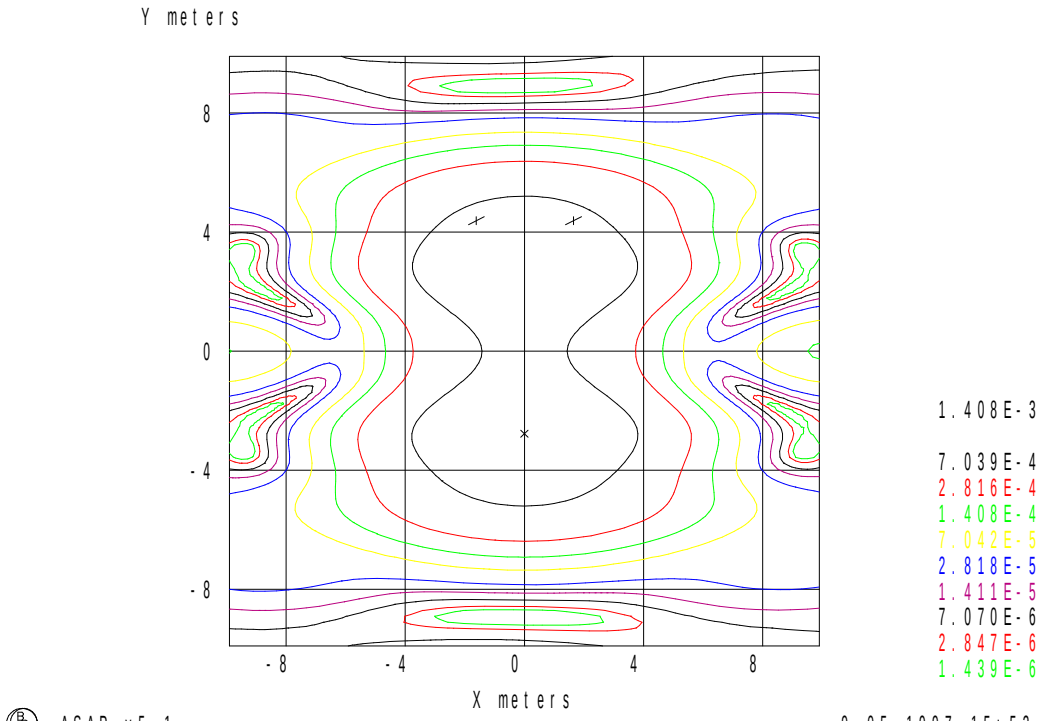

ASAP v5.1 9-05-1997 15:52

40 90 deg .0008675 .0008676 Flux/sqm 61.62497 61.6356 %

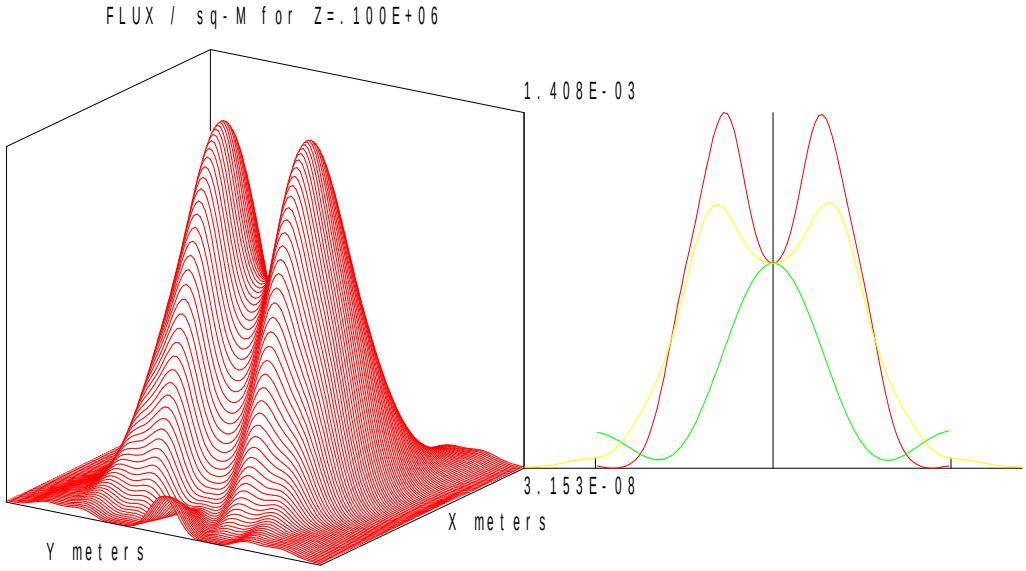

ASAP v5.1 9-05-1997 15:52

40 0 deg .0016703 .0004951 Flux/sqm 85.71449 25.40893 %

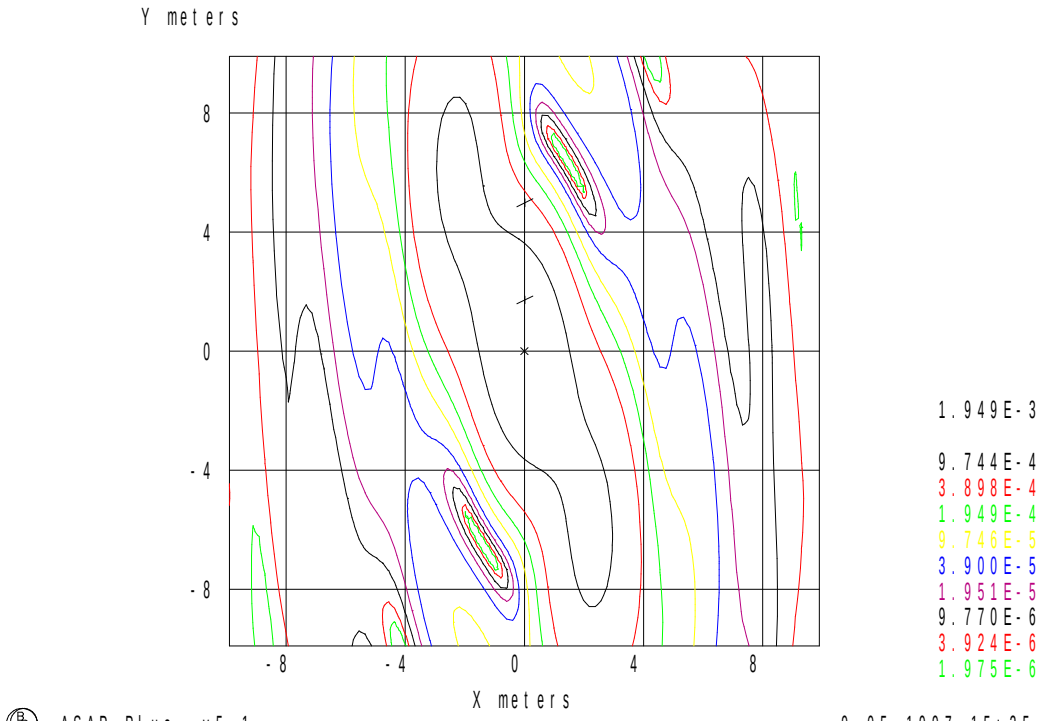

40 0 deg .0016703 .0004951 Flux/sqm 85.71449 25.40893 %